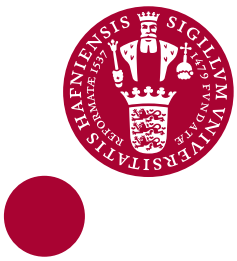

Contrasting Textural and Chemical Signatures of Chromitites in the Mesoarchaean Ulamertoq Peridotite Body, Southern West Greenland

Guotana, Juan; Morishita, Tomoaki; Yamaguchi, Ryoko; Nishio, Ikuya; Tamura, Akihiro; Tani, Kenichiro; Harigane, Yumiko; Szilas, Kristoffer; Pearson, D.

Published in:
Geosciences (Switzerland)

DOI:
10.3390/geosciences8090328

Publication date:
2018

Document version
Publisher's PDF, also known as Version of record

geosciences

MDPI

Article

Contrasting Textural and Chemical Signatures of Chromitites in the Mesoarchaean Ulamertoq Peridotite Body, Southern West Greenland

Juan Miguel Guotana [1], Tomoaki Morishita [1,*], Ryoko Yamaguchi [1], Ikuya Nishio [1], Akihiro Tamura [1], Kenichiro Tani [2], Yumiko Harigane [3], Kristoffer Szilas [4] and D. Graham Pearson [5]

1 Graduate School of Natural Science and Technology, Kanazawa University, Kanazawa, Ishikawa 920-1192, Japan; jmguotana@stu.kanazawa-u.ac.jp (J.M.G.); gucchan.kaga@gmail.com (R.Y.); ikuyanishio240@gmail.com (I.N.); aking826@staff.kanazawa-u.ac.jp (A.T.)
2 Department of Geology and Paleontology, National Museum of Nature and Science, 4-1-1, Amakubo, Tsukuba-shi, Ibaraki 305-0005, Japan; kentani@kahaku.go.jp
3 Institute of Geology and Geoinformation, National Institute of Advanced Industrial Science and Technology (AIST), Geological Survey of Japan, Central 7, 1-1-1 Higashi, Tsukuba, Ibaraki 305-8567, Japan; y-harigane@aist.go.jp
4 Department of Geosciences and Natural Resource Management, University of Copenhagen, 1350 Copenhagen, Denmark; krsz@ign.ku.dk
5 Department of Earth & Atmospheric Sciences, University of Alberta, Edmonton, AB T6G 2R3, Canada; graham.pearson@ualberta.ca
* Correspondence: moripta@staff.kanazawa-u.ac.jp; Tel.: +81-76-264-6513

Received: 29 June 2018; Accepted: 29 August 2018; Published: 3 September 2018

Abstract: Peridotites occur as lensoid bodies within the Mesoarchaean orthogneiss in the Akia terrane of Southern West Greenland. The Ulamertoq peridotite body is the largest of these peridotites hosted within the regional orthogneiss. It consists mainly of olivine, orthopyroxene, and amphibole-rich ultramafic rocks exhibiting metamorphic textural and chemical features. Chromitite layers from different localities in Ulamertoq show contrasting characteristics. In one locality, zoned chromites are hosted in orthopyroxene-amphibole peridotites. Compositional zonation in chromites is evident with decreasing Cr and Fe content from core to rim, while Al and Mg increase. Homogeneous chromites from another locality are fairly uniform and Fe-rich. The mineral chemistry of the major and accessory phases shows metamorphic signatures. Inferred temperature conditions suggest that the zoned chromites, homogeneous chromites, and their hosts are equilibrated at different metamorphic conditions. In this paper, various mechanisms during the cumulus to subsolidus stages are explored in order to understand the origin of the two contrasting types of chromites.

Keywords: chromites; compositional zonation; Greenland

1. Introduction

Several peridotite bodies enclosed in tonalitic orthogneiss are found in the Mesoarchaean Akia terrane in Southern West Greenland, which is part of the North Atlantic Craton [1]. However, the origin of these peridotite bodies is still enigmatic. The Ulamertoq body forms part of a series of lens-shaped peridotite bodies that occur in the Akia terrane, and also contains chromitite layers. Chromitites from two localities within the Ulamertoq peridotite body exhibit contrasting petrological and geochemical characteristics.

The composition of unaltered chromites has been regarded as a useful petrogenetic indicator [2–6]. However, chromite composition can be modified as a result of late-stage re-equilibration during post-accumulation [7,8], metamorphism, and hydrothermal alteration. The aforementioned processes can result in compositional zonation in chromites [9–13]. Crystal zonation can record chemical evolution, which provides vital information in reconstructing the pressure-temperature (P-T) history of the rocks [14–17]. Such compositional zonation was observed in chromitites from the western part of central Ulamertoq, wherein chromites are characterized by Cr and Fe-rich cores with Al and Mg enrichment toward the rim. Cr-rich overgrowths are commonly observed at the outermost rims. In contrast, the chromitite recovered from the eastern portion is characterized by homogenous Fe-rich chromites. In this study, possible mechanisms to explain the origin of the two types of chromitites in Ulamertoq are investigated.

2. Geological Setting

The Archaean craton of southern West Greenland can be subdivided into several tectono-magmatic terranes [18]. For the Nuuk region, the relevant terranes are the Akia, Akulleq, and Tarsiusarsuaq, from north to south (Figure 1A) [19,20]. The Archaean North Atlantic Craton is bounded by Proterozoic orogens known as the Nagssugtoqidian (north) and Ketilidian (south) [21]. The Fiskefjord area in the central Akia terrane is dominated by amphibolites, dioritic to tonalitic orthogneisses, and peridotites. The peridotites occur as large discontinuous lensoid bodies within tonalitic orthogneiss. Exposures of these peridotites can be found in the Miaggoq, Seqi, Ulamertoq, and Amikoq ultramafic bodies, which are also associated with noritic rocks [1] (Figure 1B).

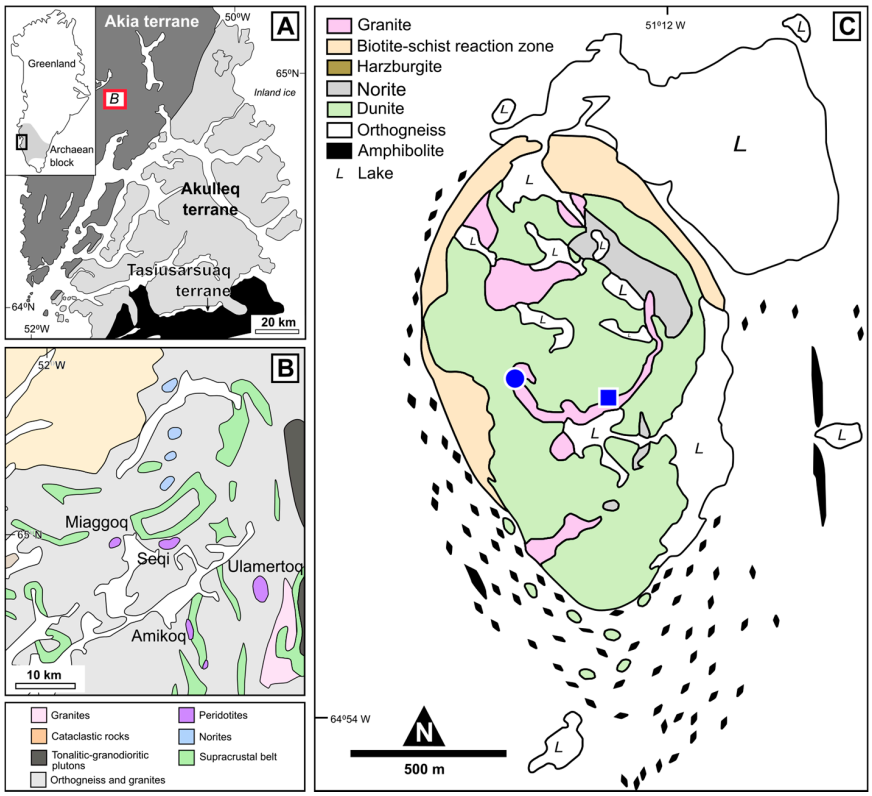

Figure 1. (**A**) Simplified geotectonic map of southern West Greenland showing the Akia, Akulleq, and Tarsiusarsuaq terranes; (**B**) Ultramafic bodies within the Mesoarchaean orthogneiss in Akia terrane (map modified from Geological Survey of Denmark and Greenland (GEUS) and Szilas et al. [22]); (**C**) Geologic map of Ulamertoq peridotite body showing the sampling locations of chromitites with zoned chromites (filled circle) and homogeneous chromites (filled square) (adapted from Garde [21]).

The Ulamertoq peridotite body measures about 1 km × 1.5 km. The immediately surrounding orthogneiss host also includes smaller pods of amphibolite, as well as peridotite (Figure 1C). The Ulamertoq peridotite body is dominated by olivine-rich plutonic rocks containing orthopyroxene and amphibole, which is similar to the other ultramafic bodies in the Akia terrane. The lithological contacts are gradational to uncertain. It is interesting to note that some Ulamertoq samples contain clinopyroxenes, which are not common in other peridotite bodies in the Akia terrane. Anthophyllite, tremolite, chlorite, and phlogopite veins are common. Chromitites occur as irregular and discontinuous layers or thin seams. Harzburgites with poikilitic orthopyroxenes are exposed in the northeastern part. The harzburgites are bounded to the northeast by medium to coarse-grained norite comprised of plagioclase, orthopyroxene, and accessory hornblende and phlogopite. These lithologies have gradational contacts. The peridotite body also has irregular sheets and pods of pink granite, which also cuts the surrounding gneiss [21,22]. The lithologies in Ulamertoq are comparable to those found in the Seqi ultramafic complex (pyroxene-amphibole peridotites or amphibole harzburgites), and tend to occur randomly [22]. The classification used by Szilas et al. [22] to refer to olivine-rich rocks with varying amounts of orthopyroxene and amphibole is also adopted. The ultramafic host and envelope will be simply referred to as peridotites hereafter.

3. Data and Results

3.1. Petrography

The chromitites sampled from the two localities in Ulamertoq (blue symbols in Figure 1C) are differentiated based on the textural and chemical characteristics of its constituent grains, as zoned and homogeneous chromites. The zoned chromites are characterized by concentric zonation with gradually decreasing Cr and Fe concomitant with increasing Mg and Al from core to rim. The homogeneous chromites have fairly uniform composition from core to rim. The peridotite envelope and host of the two types of chromitites also have contrasting features, which will be discussed below.

3.1.1. Zoned Chromite

Chromitites that contain zoned chromites have massive texture. The chromites occur as subhedral to euhedral grains (up to 500 μm). Zonations are observed in backscattered electron (BSE) images, which show concentric variation from bright cores to dark rims. The contrast from core to rim observed in BSE images can be correlated with compositional variation (Section 4.2) (Figure 2C,D and Figure 3). The cores of the zoned chromites are Cr- and Fe-rich, which decrease steadily toward the rim. In contrast, the concentrations of Al and Mg progressively increase away from the core. Thin overgrowths having intermediate composition relative to the core and rim appear as irregular light gray "outer rims" in the BSE images (Figure 2C,D). The outer rims have sharp contacts with the dark rims of the zoned chromites. Zonation is clearer in coarser chromite grains than in finer grains. Chromite core chemistry was analyzed from the brightest portion of a grain (BSE images), and shows a wide range of compositions within a single thin section. Inclusions in the chromites are mainly amphibole, orthopyroxene, and chlorite, which also commonly occur as interstitial minerals between chromites (Figure 2A–D). The portions within chromite enclosing the silicate inclusions are dark in the BSE images, suggesting that the composition of chromite is affected by the included and surrounding silicate phases. Elemental diffusion in the presence of Al-rich phases has been demonstrated by previous studies on zoned chromites from other localities (e.g., Red Mountain in New Zealand [23]; Rhum layered intrusion in Scotland [7], and the Yanmenguan mafic-ultramafic complex in China [24]). The peridotite envelope and host consist mainly of olivine, orthopyroxene, magnesiohornblende, phlogopite, and accessory chromite (Figure 2E–G). The accessory chromites in the peridotite envelope are also zoned similar to those in the chromite-rich zone. However, accessory chromites in the host have different textures that are more irregular to subhedral with Cr-rich thin rims (Cr# = 0.37–0.58). The chromite rims have porous textures and contain fine chlorite inclusions (Figure 2C).

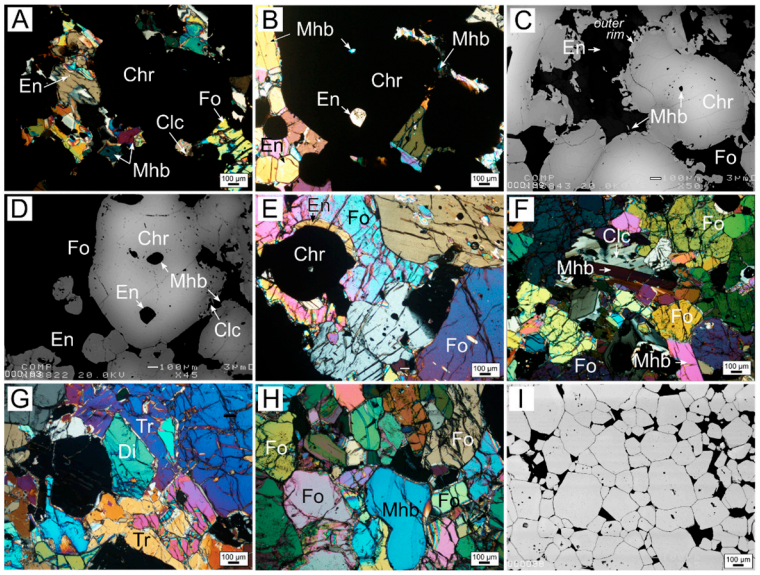

Figure 2. (**A**,**B**) Photomicrographs of samples with zoned chromites (Chr) showing interstitial silicate minerals that include enstatite (En), magnesiohornblende (Mhb), forsterite (Fo), and clinochlore (Clc); (**C**,**D**) Backscattered electron (BSE) images of the zoned chromites showing a gradual change from bright cores to dark rims. Outer rims occur as irregular overgrowths and have sharp contacts with dark rims; (**E**,**F**) Photomicrographs of the peridotite envelope (**E**) and host (**F**) of the chromitite hosting zoned chromites; (**G**,**H**) The peridotite host of the homogeneous chromites lacks orthopyroxenes, but contains diopside (Di) and tremolite (Tr); (**I**) BSE image of the homogenous chromite shows uniform brightness from core to rim.

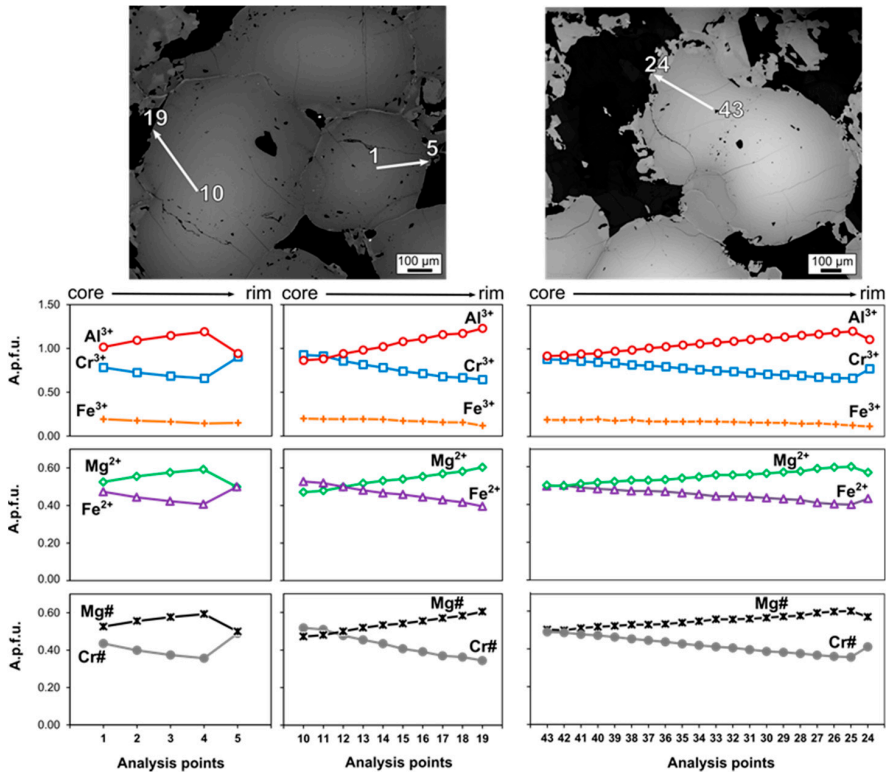

Figure 3. Line analyses of zoned chromite grains showing a decrease of Cr and Fe coupled with Al and Mg enrichment from core to rim (a.p.f.u., (atoms per formula unit) for O = 4). Typical outer rims are Cr-rich and Al-depleted (shown as analysis point no. 24).

Olivine in the peridotite envelope and host occurs as large crystals (approximately 1.5–6.5 mm), which sometimes contain orthopyroxene and amphibole inclusions. Most of the coarse olivine grains contain minute opaque inclusions, which are probably magnetites (Figure 2E,F). Finer euhedral olivine grains with well-formed polygonal crystal boundaries are also present. These finer olivine grains are clear and appear to be forming a vein-like fabric. Orthopyroxenes are mainly enstatite ($En_{89–91}$), and are the only pyroxene phase observed in the chromitites with zoned chromites, envelope, and host peridotites. Exsolution lamellae of clinopyroxene were not observed in any of the orthopyroxenes from the studied samples. In some portions, orthopyroxenes occur adjacent to chromites, forming sutured contacts with chromites (Figure 2E). Amphiboles are commonly anhedral to subhedral, and are closely associated with intergranular orthopyroxenes and chlorite in the chromitites. In the peridotite host, amphiboles are commonly found as discrete grains between olivine and orthopyroxenes (Figure 2F).

3.1.2. Homogeneous Chromites

Chromitites with homogeneous chromites are closely packed, and have a low proportion of interstitial phases. These chromites are also finer (up to 200 μm) and exhibit equilibrium textures. Inclusions are also fewer and finer compared to the zoned chromites. Chromites within the chromitite have fairly uniform composition from core to rim. Intergranular phases include olivine, amphibole, and chlorite (Figure 2G,I). Clinopyroxenes are only observed in chromitite with homogeneous chromites. The clinopyroxenes are also free of exsolution lamellae. The envelope adjacent to the chromite-rich zone contains clinopyroxenes that are closely associated with tremolite (Figure 2G). Clinopyroxenes and amphiboles are more abundant around the chromite-rich zones. The amount of olivine also increases toward the host as you go away from the chromite-rich zone. Tremolite commonly encloses clinopyroxene, and also occurs as prismatic grains.

4. Mineral Chemistry

4.1. Analytical Methods

Major-element compositions of minerals were obtained using a JEOL JXA-8800 (Jeol Ltd., Akishima, Tokyo, Japon) electron probe microanalyzer (EPMA) at the Kanazawa University with operating conditions of 20-kV accelerating voltage, 20-nA beam current, and a 3-μm beam diameter. Natural and synthetic standards were used throughout the analysis. ZAF (Z = atomic number, A = absorption, F = characteristic fluorescence) correction using JEOL JXA-880 software was also used in data processing. Representative major element compositions are presented in Supplementary Tables S1–S8.

Rare earth element (REE) and trace element compositions of amphiboles and clinopyroxenes were determined using a Laser Ablation Inductively Coupled Plasma Mass Spectrometry (LA-ICP-MS) (Agilent 7500S equipped with MicroLas Geolas Q-plus laser system; Agilent Technologies, Santa Clara, CA, US) at Kanazawa University. Each analysis was performed by an ablating spot of 50 μm in diameter at a repetition rate of 6 Hz. NIST SRM 612 was used as an external reference material [25], and data reduction was facilitated using ^{29}Si as the internal standard, based on the SiO_2 content obtained by EPMA [26]. The complete details of the analytical methods and conditions are described by Morishita et al. [27,28]. Representative REE and trace element compositions are listed in Supplementary Table S9.

4.2. Chromite

The chromites in the zoned chromitites have a varying core to rim composition. Their cores are characterized by Cr# [(Cr/Cr + Al) atomic ratio] ranging from 0.32 to 0.62, Mg# [(Mg/Mg + Fe^{2+}) atomic ratio] between 0.4 and 0.6, Al_2O_3 varying from 18.0 wt % to 34.9 wt %, TiO_2 content ranges from 0.11 wt % to 0.17 wt %, and FeO* (=FeO total) ranging from 22.4 wt % to 28.6 wt %. The rims of the zoned chromites have lower Cr# (0.34–0.49), higher Mg# (0.50–0.59), higher Al_2O_3 (25.1–34.9 wt %),

lower TiO_2 (0.07–0.14 wt %), and lower FeO* (21.4–25.8 wt %). Proportions of Fe^{2+} and Fe^{3+} were calculated based on stoichiometry. The Fe^{2+} and Fe^{3+} contents decrease from core to rim and increase in the outer rims (Figure 3). The thin and irregular-shaped outer rims occur as overgrowths, and are compositionally different (Cr# = 0.37–0.58) from the dark rims with Al_2O_3 contents from 21.2 wt % to 35.2 wt %, TiO_2 varying from 0.04 wt % to 0.14 wt % and FeO* from 20.4 wt % to 26.3 wt % (Figure 4A). The accessory chromites in the peridotite immediately adjacent to the chromitites (envelope) also show similar Cr and Fe depletion with Al and Mg enrichment from core to rim. The same zonation is not observed with the accessory chromite in the peridotite host, which is characterized by Cr enrichment from core to rim.

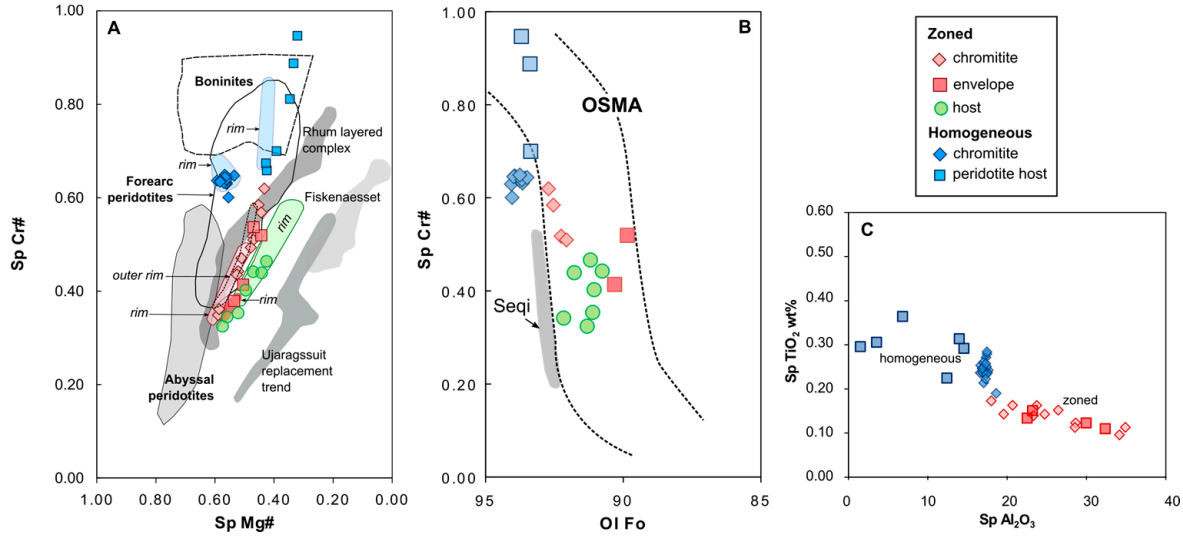

Figure 4. (**A**) Spinel Mg# [(Mg/Mg + Fe^{2+}) atomic ratio] vs. Cr# [(Cr/Cr + Al) atomic ratio] plot showing higher and less variable Cr# and Mg# for the homogeneous chromites, while zoned chromites have a wide range of Cr# and Mg#. However, the accessory chromites in the peridotite host have higher Cr#; (**B**) Forsterite content vs. Cr# of olivine–spinel pairs of the Ulamertoq samples. Fields of the olivine–spinel mantle array (OSMA) [4] and Seqi ultramafic complex [1] are shown for reference; (**C**) The homogeneous chromites are characterized by higher TiO_2 contents compared to the zoned chromites. Fields for Rhum layered complex [29], Ujaragssuit [30], and Fiskenaesset [31] are included for comparison.

Homogeneous chromites have a narrow range of Cr# from 0.60 to 0.65, Mg# from 0.54 to 0.59, Al_2O_3 varying from 16.6 wt % to 18.6 wt %, TiO_2 varying from 0.19 wt % to 0.28 wt %, and FeO* varying from 22.9 wt % to 25.03 wt % (Figure 4A–C).

4.3. Olivine

The interstitial olivine grains around the zoned chromites have a limited range of forsterite contents (Fo = 100 × Mg/Mg + Fe^{2+}) from 92.1 to 93.7 wt %) (Figures 4B and 5A) and NiO contents (0.37–0.43 wt %). The peridotite envelope and host have lower olivine Fo contents (Fo = 89.9–92.2 wt % and 90.4–90.5 wt %) and olivine NiO contents (NiO = 0.28–0.37 wt % and 0.29–0.34 wt %) (Figure 5A).

The olivine grains interstitial to the homogeneous chromites and those within its host have a narrow range of forsterite contents (Fo = 93.5–94.1 wt % and 93.4–93.7 wt %, respectively) which is higher than those associated with zoned chromites. It is also shown in the OSMA (olivine–spinel mantle array) diagram [4] that the olivine forsterite content in the sample with homogenous chromites is slightly higher relative to those with zoned chromites, as also shown in Figure 4B. The olivine NiO content values related with the homogeneous chromites (0.31–0.44 wt %) are comparable to

those with the zoned chromites (Figure 5A). The olivine MnO contents in both types of chromites are almost similar.

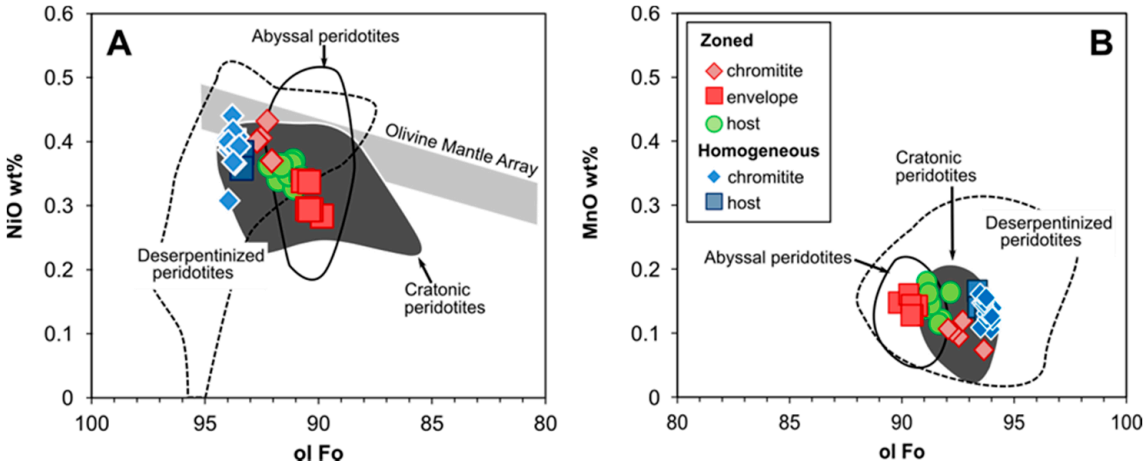

Figure 5. (**A**) Olivine forsterite content vs. NiO wt % plot of the Ulamertoq samples. Compositional fields of other metamorphic olivine and residual mantle olivine from typical abyssal peridotites and cratonic spinel-facies peridotites [29–32] are also plotted. The mantle olivine array is from Takahashi et al. [33]; (**B**) The olivine forsterite content and MnO wt % of the Ulamertoq samples are compared with other metamorphic olivine from various studies and olivine from typical residual abyssal peridotite from Warren [34]. Compositions of metamorphic olivine from the Happo-O'ne peridotite complex [35], Tari-Misaka [36], Ohsa-Yama [37] in Japan, and abyssal peridotites [34] are also included for comparison.

4.4. Pyroxenes

The Mg# and Cr_2O_3 contents of the orthopyroxenes (enstatite) in the chromitites with zoned chromites (0.91, 0.20–0.37 wt %, respectively) and those within the peridotite host (0.91, 0.21–0.30, respectively) are slightly higher compared to those from the peridotite envelope (0.90, 0.12–0.19, respectively). The orthopyroxene Al_2O_3 content is also low (1.2–1.9 wt %). Clinopyroxenes associated with the homogeneous chromites and its peridotite host also have low Al_2O_3 contents (0.32–0.68 wt %) with a wide-ranging Cr_2O_3 (0.00–0.17 wt %) and less variable Mg# (0.96–0.97) (Figure 6C,D).

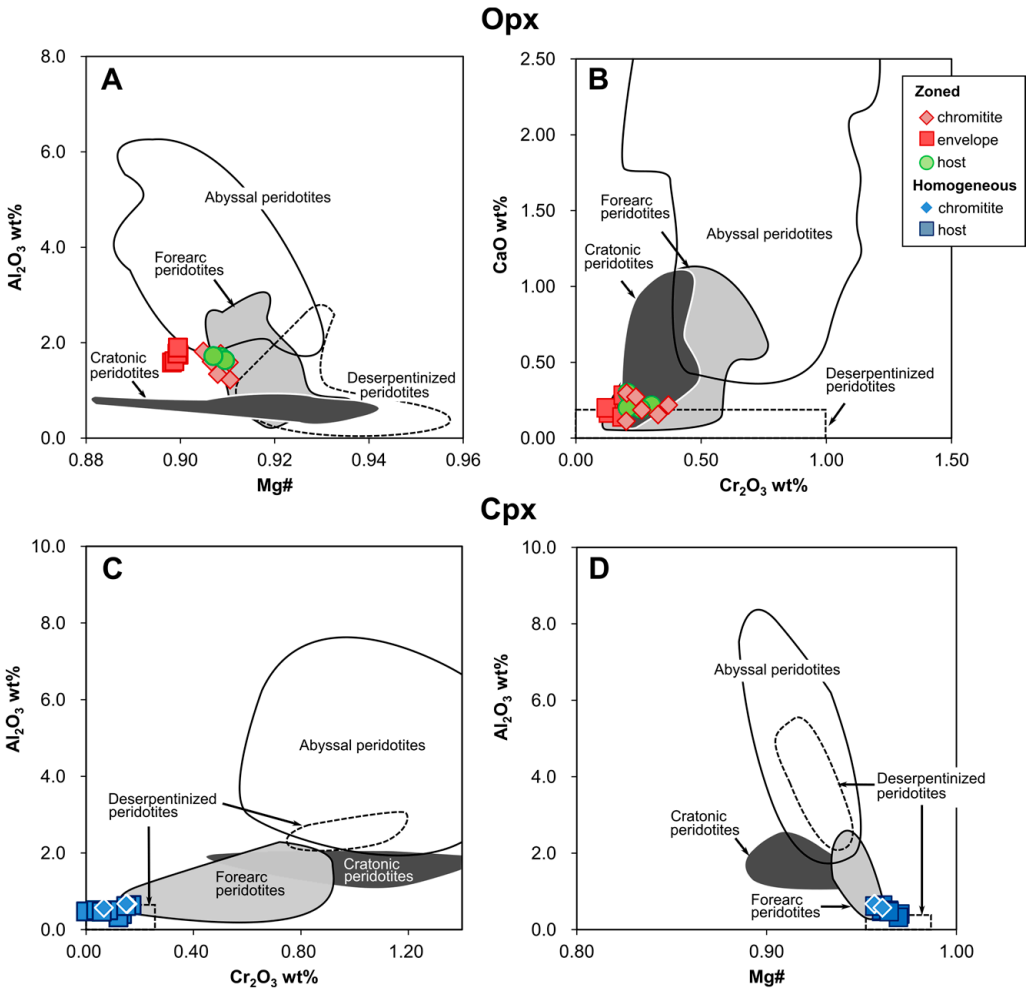

Figure 6. (**A**) Mg# vs. Al_2O_3 wt % and Cr_2O_3 wt % vs. CaO wt % plots of orthopyroxenes (Opx); (**B**) Mg# vs. Al_2O_3 wt % and Cr_2O_3 wt % vs. Al_2O_3 wt % of the clinopyroxenes (Cpx). Compositions of metamorphic olivine from the Happo-O'ne peridotite complex [35], Tari-Misaka [36], Ohsa-Yama [37] in Japan, abyssal peridotites [34], and cratonic peridotites [38] are also included for comparison.

4.5. Amphibole

Amphiboles in both types of chromitites and their peridotite hosts are mainly magnesiohornblende [Mg# = 0.90–0.96, Si a.p.f.u. (atoms per formula unit) = 6.79–7.48 (a.p.f.u. for O = 23)]. Tremolites were only observed in the homogeneous chromitites and its peridotite host with higher Mg# (0.95–0.97) and Si a.p.f.u. (7.53–7.93) (Figure 7).

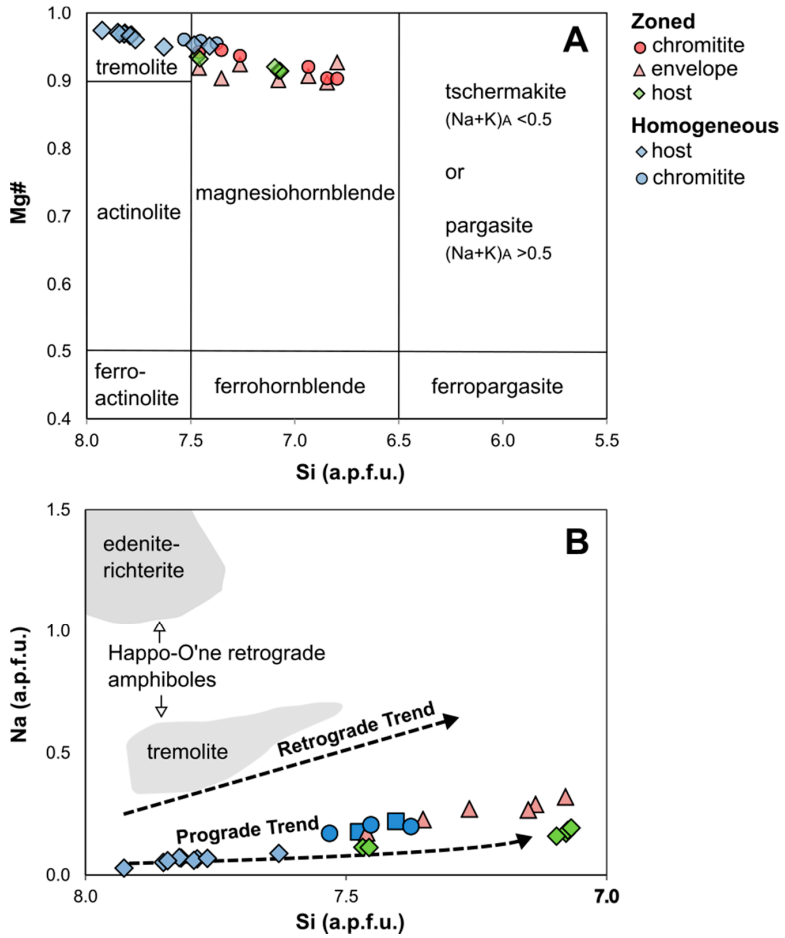

Figure 7. (**A**) Classification of amphibole based on Si atoms per formula unit (a.p.f.u.). and Mg# [39]; (**B**) Si a.p.f.u. vs. Mg# of tremolites and amphiboles from Ulamertoq samples. Prograde and retrograde trends of tremolites are from the study of Nozaka in the Happo ultramafic complex [40]. Retrograde amphibole fields are from the study of Khedr and Arai [35].

4.6. Trace Element Geochemistry of Amphiboles and Clinopyroxenes

Amphiboles in both studied chromitites are slightly enriched in light REEs relative to heavy REEs ($[Ce/Yb]_N$ = 1.46–3.33). As shown in Figure 8A, in the trace element patterns of hornblende in the zoned chromitite, Sr and high field strength elements (HFSE: Ti, Zr, Nb, and Ta) exhibit various degrees of negative anomalies relative to neighboring REEs. In the homogeneous chromitite (Figure 8B), trace element abundances are clearly lower in tremolite (e.g., Yb_N = 4.29) than in hornblende (e.g, Yb_N = 6.60–13.18). The REE patterns of the hornblende and tremolite are characterized by obvious negative Eu anomalies in contrast to those of hornblende in the chromitite hosting zoned chromites. In the trace element patterns, Sr and HFSE exhibit strong negative anomalies (Figure 8B). The REE compositions of clinopyroxene are almost equivalent to that of tremolite related to the homogeneous chromites. The clinopyroxenes associated with the homogeneous chromites are depleted in Sr, Eu, and HFSE (Ti, Zr, and Ta).

Amphiboles show similar patterns in the chondrite-normalized spider diagram, with a more pronounced Sr anomaly compared to the clinopyroxenes (Figure 8).

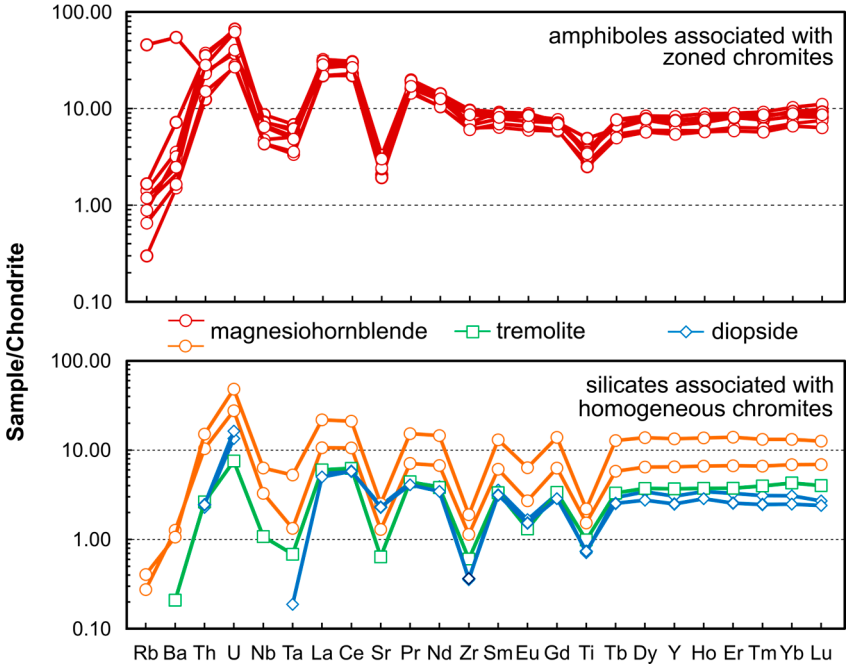

Figure 8. Chondrite-normalized trace element concentration of the amphiboles and clinopyroxenes of the Ulamertoq samples. Normalizing values are from Sun and McDonough [41].

5. Discussion

5.1. Original Composition of Zoned Chromites

The cores of the zoned chromites show a wide variety of chemical compositions. The core compositions from different grains have a broad range of Cr# aside from the individual variation within each grain. Therefore, the original composition of the chromites may not be preserved by most of the chromite cores. The most Cr-rich cores of the zoned chromites are comparable to the homogeneous chromites. Chromite cores with the highest Cr content could have possibly retained the original composition of the zoned chromites. Some of these chromite grains, with relatively higher Cr#, are partly or entirely enclosed within olivine. Chromites that are closely associated with olivine show lesser variation in composition from core to rim (Figure 9). The surrounding olivine may have buffered the trivalent cation diffusion with chromite, because it contains lesser Al, Cr, and Fe^{3+}. This observation is also similar to the accessory spinels in the ultramafic rocks from the Yanmenguan mafic-ultramafic complex [42]. In comparison to the chromites enveloped by Al-rich phases, the core compositions of some of the chromites surrounded by olivine may be the least modified. Core compositions of such zoned chromites are characterized by higher Cr content (Cr# = 0.52–0.62) relative to other zoned chromite grains (as low as Cr# = 0.35) that are surrounded by Al-rich phases. Those chromites enveloped by olivine, which are also the most Cr-rich, could possibly represent the original composition of the chromites. Although, the possibility that the original chromite composition may have completely overprinted is also not ruled out.

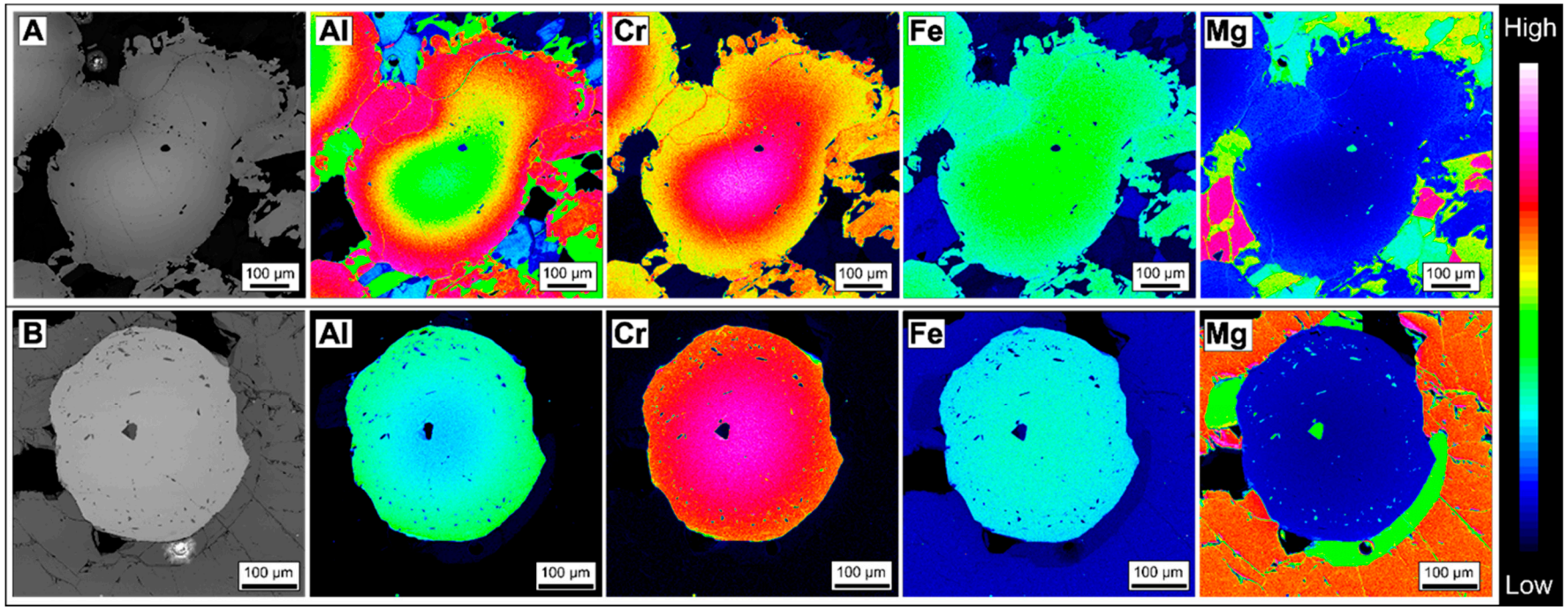

Figure 9. Backscattered electron images and false-color compositional maps of zoned chromites from the Ulamertoq peridotite body. (**A**) Chromite surrounded by chlorite, amphibole, and orthopyroxene showing a well-defined zonation of a Cr-rich core and Al-rich rims. Some chlorites fill the pores in the outer rim portions. The outermost rim occurs as irregular overgrowth, and is slightly Cr-rich; (**B**) Accessory chromite in the peridotite envelope enclosed by olivine and minor orthopyroxene shows less variation from core to rim.

It is obvious that zoned chromites were chemically modified from the original igneous compositions. Core analyses exhibit a wide variety of Al contents from core to rim, and among chromite grains in a single thin section (Figure 10). Moreover, coarser chromite grains tend to retain a more pronounced compositional zonation, whereas finer grains are more readily equilibrated with surrounding silicate phases. These observations further complicate the possible original composition of chromites.

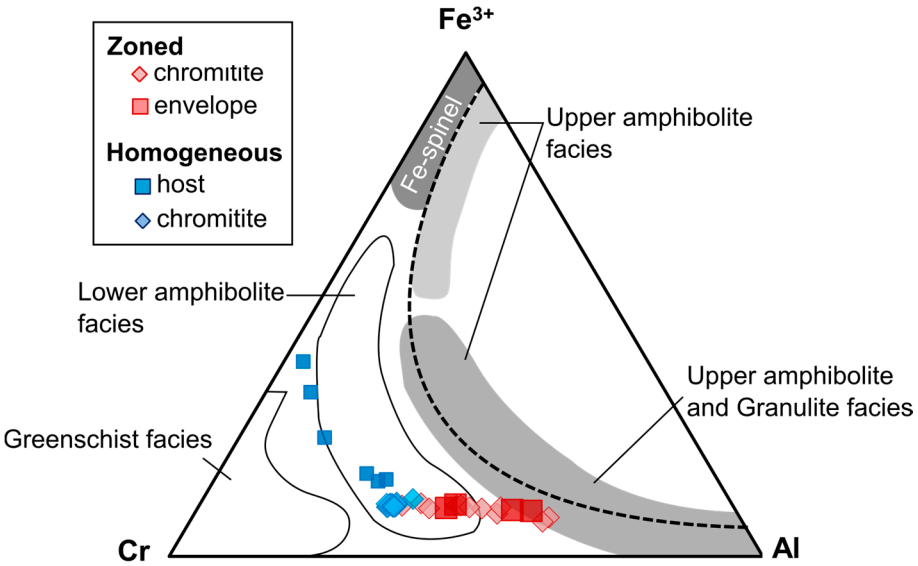

Figure 10. Cr–Fe^{3+}–Al triangular plot of the Ulamertoq chromites with fields of metamorphic spinels from different metamorphic grades (fields taken from the data of Purvis et al. [43], Evans and Frost, [9], and Suita and Streider [44]).

The TiO_2 and Al_2O_3 of the melt from which the chromites crystallized are highly associated with the TiO_2 and Al_2O_3 of the chromites [6,24]. The composition of the Ulamertoq chromites suggests that the zoned chromites, if retaining igneous compositions, formed from a melt with higher Al_2O_3 and lower TiO_2 melt, in contrast to the homogeneous chromite (Figure 4C).

5.1.1. Chromite Composition Variation

Compositional variations within chromite grains may be associated with the changes in the parental melt [45]. The depletion of Cr in the residual melt as a result of extensive chromite crystallization could produce a more Cr-poor and Al-rich melt [45,46]. The change in melt composition during crystallization could also affect the chromite composition. This mechanism of progressive change from a Cr-rich core to Al-rich rim was observed in layered mafic-ultramafic complexes (e.g., the Rhum layered mafic-ultramafic complex) [46,47]. The spinel chemistry of the peridotites from the Rhum layered complex (Scotland) [46] and Red Mountain (New Zealand) [23] also show an increase in Mg and Al, and a decrease in Cr and Fe, from core to rim. The compositional changes within chromite grains were attributed to the postcumulus reaction of chromite with intercumulus liquid and Al-rich cumulus phases. Similar chromite zonation was also observed in cumulates from the Bushveld complex (South Africa), but it was linked to reactions during the cumulus stage at the onset and early stages of chromite crystallization [48].

Subsolidus elemental exchange between chromite and coexisting Al-rich phases could also account for the zonation observed in the chromites [49]. The compositional zonation observed in the chromites that are closely associated with pyroxenes, amphiboles and plagioclase from the Red Mountain mafic-ultramafic complex and Rhum layered complex are also attributed to subsolidus reactions. Continuous elemental exchange from postcumulus to subsolidus stages may have caused

the Al enrichment along the chromite rims. In the Yanmenguan mafic-ultramafic complex in China, similar zonations characterize the chromite inclusions in enstatite, tschermakite, and phlogopite [42]. Olivine-hosted chromites also exhibit zonation, but to a lesser extent due to its low Cr and Al contents relative to pyroxenes and amphiboles.

Another mechanism that may explain the enrichment of Al toward the rim in chromite is its reaction with surrounding chlorite, as observed in the Calzadilla de los Barros ultramafic body (Spain). In a retrograde P-T path, chromite and olivine with high silica activity and a high fluid-to-rock ratio result in the formation of chlorite and Al-poor chromite [13]. Subsequent heating, which may have been caused by the gabbro intrusions in the area, initiated a reaction in the opposite direction. The reaction of chlorite and chromite at a higher temperature resulted in an increase of Mg and Al in the chromites at Calzadilla de los Barros [50].

5.1.2. Metamorphism vs. Metasomatism

Diopsides have compositions that are different from typical primary residual clinopyroxenes. Tremolite surrounding the diopside displays a replacive texture (Figure 2G). Trace element data show that the tremolites and magnesiohornblendes have trace element patterns similar to the clinopyroxenes, but are relatively more enriched, suggesting the possible effects of metasomatism. The presence of phlogopite in the samples with zoned chromitites hints at the introduction of K from metasomatizing fluids, or melts that could probably be associated with the tonalitic gneiss enclosing and intruding the peridotite bodies.

5.1.3. Metamorphism and Pressure-Temperature Path

Several textural and chemical features of the peridotite envelope and host represent metamorphic imprints on the Ulamertoq peridotite body. The variable compositions of the chromite cores, with a significant increase in Al and Mg coupled with Cr and Fe^{2+} decrease from core to rim, suggest that the Ulamertoq chromitites were modified under prograde metamorphism. Chromites that were metamorphosed at low temperatures typically have low Al contents [51]. Metamorphic reactions above 550 °C with surrounding silicates and infiltrating fluids will modify the trivalent cation chemistry of the chromites [52,53]. Comparison with other metamorphic spinels from various metamorphic grades places the zoned chromites from Ulamertoq between the fields of lower amphibolite and upper amphibolite–granulite facies (Figure 10).

Silicate phases in the peridotite envelope and host show textural and compositional characteristics affected by metamorphism. Most of the olivine grains contain minute opaque inclusions that can be attributed to the deserpentinization process [36]. The dehydration of serpentine during prograde metamorphism produces Mg-rich metamorphic olivine and Fe-rich opaque phases [36,54]. The dehydration of serpentine and recrystallization of secondary olivine could explain the abundance of such inclusions. This process could also be linked to the MnO enrichment in olivine, in which it is preferentially partitioned. Also, the depletion of Al_2O_3 in the pyroxenes has been ascribed to a metamorphic or secondary origin (Figure 6A–D) [36,55]. Low CaO, Al_2O_3, and Cr_2O_3 in the orthopyroxenes are commonly observed in metasomatic orthopyroxenes in deserpentinized peridotites [56]. Secondary orthopyroxenes can be formed by the reaction between Si-rich melt/fluid with olivine [57]. The composition of the tremolites and other amphiboles are also similar to prograde tremolites that are interpreted as products of the breakdown of serpentine [35,40].

The silicates that are interstitial to the zoned chromites and within the peridotite envelope include olivine+orthopyroxene+amphibole. In the CaO-MgO-SiO_2-H_2O phase equilibria, this assemblage is stable above 650 °C. However, the absence of clinopyroxene from this sample limits the temperature to below 800 °C [58]. Orthopyroxenes in prograde metamorphism may be produced by the reaction: 2Tlc + 2Fo = 5En + 2H_2O (Tlc = talc; Fo = forsterite; En = enstatite) (Figure 11).

The Al increase toward the rim can be explained by the reaction of chromite with Al-rich silicates driven by high-grade metamorphism [9]. The outer rims of the zoned chromites preserve porous

textures with chlorite inclusions. The Cr# increases and Al content decreases in the outermost rims. The outer rims could be products of equilibration during a retrograde stage in the presence of fluids. The outer rims that are commonly in contact with chlorite could be products of a younger event.

The chromitite with homogeneous chromites and its peridotite envelope contain clinopyroxenes, but are devoid of orthopyroxene. The assemblage olivine+clinopyroxene+tremolite suggests a lower temperature stability at around 530 °C [58]. Clinopyroxene may also be stable at higher temperatures, but the absence of orthopyroxene points more likely to a lower temperature stability.

The similarity of REE patterns between clinopyroxenes and amphiboles possibly indicates strong modification by a hydrous melt [59,60] during metamorphism, which is also suggested by their textural relationship.

The absence of plagioclase and garnet restricts the pressure of the Ulamertoq ultramafic rocks within the spinel stability field. The transition from plagioclase to spinel in lherzolites occurs within 0.6–0.8 GPa [61–63], and spinel-to-garnet lherzolite transitions at 3.0 GPa, depending on the Cr# of the system [64,65]. Hence, the equilibration temperature condition of the Ulamertoq peridotite may be between these transition pressures. Pressure constraints may only be based on the presence of chromite in the spinel stability field, although the possibility of coexistence of the assemblages in both types of chromitites and associated peridotites above 14 kbar (CaO-MgO-SiO_2-H_2O phase equilibria) is not disregarded (Figure 11).

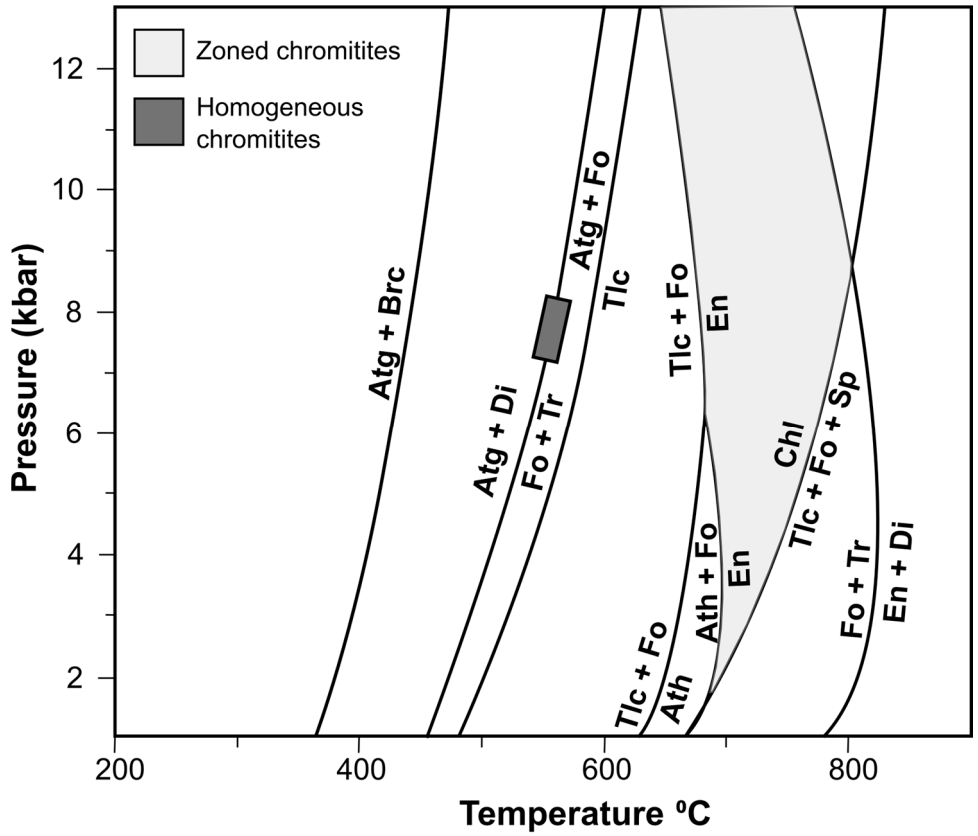

Figure 11. CaO-MgO-SiO_2-H_2O phase equilibria of ultramafic rocks [66,67]. Abbreviations: Atg = antigorite, Brc = brucite, Di = diopside, Fo = Forsterite, Tr = tremolite, Tlc = talc, Ath = anthophyllite, Chl = chlorite, Sp = spinel, En = enstatite.

5.1.4. Ulamertoq Peridotites: Mantle Residue or Cumulate?

It is possible that the Fiskefjord peridotite bodies may represent residues after extensive melt extraction; however, a cumulate origin is currently favored [22]. Bulk-rock geochemistry shows

that the MgO contents of the Seqi peridotites are compositionally variable, extending up to 50%, and FeO_t is too high for typical mantle rocks [68]. The mantle-derived ultramafic rocks erupted by kimberlites in southern West Greenland typically are relatively orthopyroxene-poor, and have orthopyroxene compositions that are consistent with equilibration pressures ranging from the spinel to garnet stability fields [38,69]. Furthermore, the close spatial association of the Fiskefjord peridotites with norites is consistent with their origin as fragments of layered complexes that predate the regional tonalitic orthogneiss [1]. Several lines of petrological, field, and geochemical evidence also favor a cumulate origin. The presence of poikilitic pyroxenes and reports of chromitites occurring as subparallel layers, orthopyroxene cross-bedding, and layering in the field are more associated with igneous crustal processes [22]. The bulk-rock chemistry of Seqi peridotites is also akin to komatiite cumulates. The spinel Mg# of the Ulamertoq is also incomparable to typical mantle rocks [68], but it is similar to those observed in Seqi peridotites (Figure 4B) that also intrude the regional orthogneiss, and are currently interpreted as an ultramafic cumulate. The Cr# also exhibits variable Al enrichment, even among core analyses, and thus not all cores are representative of its pristine composition. Norites are closely associated with the Fiskefjord peridotites [1]. In Seqi peridotites, negative Eu anomalies observed in the bulk rock, and amphibole chemistry also suggest a possible link to plagioclase fractionation with the surrounding norites. Such an anomaly was also observed in the orthopyroxenes. The Ulamertoq peridotite body is also closely associated with norites (Figure 1C).

6. Conclusions

The chromitites recovered from different localities in Ulamertoq show contrasting textural, mineralogical, and compositional characteristics. The zoned chromites are hosted in olivine-orthopyroxene-amphibole peridotite, and could be possibly metamorphosed up to upper amphibolite facies. The compositional zonation in chromites may be attributed to subsolidus equilibration with surrounding Al-rich phases. The homogeneous chromites, on the other hand, are hosted in olivine-clinopyroxene-tremolite peridotite, and could be metamorphosed at a lower metamorphic grade (greenschist to lower amphibolite facies), or have retrogressed more extensively. The presence of outer rims of Al-poor chromites may represent a younger metasomatic event involving retrograde chlorite. The composition of silicate phases also suggests metamorphic recrystallization. It is possible that several metamorphic imprints are already observed, and the detailed P-T path may be more complex. The combined petrological and mineral chemical data available for the Ulamertoq peridotite body suggest that the ultramafic rocks within it are likely derived via cumulate processes rather than the body representing a fragment of residual upper mantle.

Supplementary Materials: The following are available online at http://www.mdpi.com/2076-3263/8/9/328/s1, Tables S1–S8: Major element compositions of spinel, olivine, orthopyroxene, clinopyroxene, amphibole and chlorite, and Table S9: Trace element compositions of clinopyroxenes and amphibole.

Author Contributions: T.M., K.S., D.G.P., I.N. and K.T. conducted field surveys in southern West Greenland and provided insights on how to improve the manuscript. R.Y., I.N., Y.H., J.M.G. and A.T. analyzed chemical compositions of minerals. J.M.G. prepared the manuscript.

Funding: This study was financially supported by a Grant-in-Aid for Scientific Research of the Ministry of Education Culture, Sports, Science and Technology of Japan (No. 16H05741: TM). K.S. acknowledges the Carlsberg Foundation for financial support of the fieldwork in Greenland to collect the Ulamertoq samples.

Acknowledgments: We are grateful to S. Umino and T. Mizukami for the discussions during the manuscript preparation.

Conflicts of Interest: The authors declare no conflict of interest. The founding sponsors had no role in the design of the study; in the collection, analyses, or interpretation of data; in the writing of the manuscript, and in the decision to publish the results.

References

1. Szilas, K.; Kelemen, P.B.; Bernstein, S. Peridotite enclaves hosted by Mesoarchaean TTG-suite orthogneisses in the Fiskefjord region of Southern West Greenland. *GeoResJ* **2015**, *7*, 22–34. [CrossRef]

2. Irvine, T.N. Chromian spinel as a petrogenetic indicator: Part 2. Petrologic applications. *Can. J. Earth Sci.* **1967**, *4*, 71–103. [CrossRef]
3. Dick, H.J.B.; Bullen, T. Chromian spinel as a petrogenetic indicator in abyssal and alpine-type peridotites and spatially associated lavas. *Contrib. Mineral. Petrol.* **1984**, *86*, 54–76. [CrossRef]
4. Arai, S. Characterization of spinel peridotites by olivine-spinel compositional relationships: Review and interpretation. *Chem. Geol.* **1994**, *113*, 191–204. [CrossRef]
5. Barnes, S.J.; Roeder, P.L. The range of spinel compositions in terrestrial mafic and ultramafic rocks. *J. Petrol.* **2001**, *42*, 2279–2302. [CrossRef]
6. Kamenestky, V. Factors Controlling Chemistry of Magmatic Spinel: An Empirical Study of Associated Olivine, Cr-spinel and Melt Inclusions from Primitive Rocks. *J. Petrol.* **2001**, *42*, 655–671. [CrossRef]
7. Henderson, P.; Wood, R.J. Reaction relationships of chrome-spinels in igneous rocks—further evidence from the layered intrusions of Rhum and Mull, Inner Hebrides, Scotland. *Contrib. Mineral. Petrol.* **1982**, *78*, 225–229. [CrossRef]
8. Roeder, P.L.; Campbell, I.H. The effect of postcumulus reactions on composition of chrome-spinels from the jimberlana intrusion. *J. Petrol.* **1985**, *26*, 763–786. [CrossRef]
9. Evans, B.W.; Frost, B.R. Chrome-spinel in progressive metamorphism—A preliminary analysis. *Geochim. Cosmochim. Acta* **1975**, *39*, 959–972. [CrossRef]
10. Proenza, J.A.; Ortega-Gutiérrez, F.; Camprubí, A.; Tritlla, J.; Elías-Herrera, M.; Reyes-Salas, M. Paleozoic serpentinite-enclosed chromitites from Tehuitzingo (Acatlán Complex, southern Mexico): A petrological and mineralogical study. *J. South Am. Earth Sci.* **2004**, *16*, 649–666. [CrossRef]
11. Mellini, M.; Rumori, C.; Viti, C. Hydrothermally reset magmatic spinels in retrograde serpentinites: Formation of "ferritchromit" rims and chlorite aureoles. *Contrib. Mineral. Petrol.* **2005**, *149*, 266–275. [CrossRef]
12. Merlini, A.; Grieco, G.; Diella, V. Ferritchromite and chromian-chlorite formation in mélange-hosted Kalkan chromitite (Southern Urals, Russia). *Am. Mineral.* **2009**, *94*, 1459–1467. [CrossRef]
13. Gervilla, F.; Padrón-Navarta, J.A.; Kerestedjian, T.; Sergeeva, I.; González-Jiménez, J.M.; Fanlo, I. Formation of ferrian chromite in podiform chromitites from the Golyamo Kamenyane serpentinite, Eastern Rhodopes, SE Bulgaria: A two-stage process. *Contrib. Mineral. Petrol.* **2012**, *164*, 643–657. [CrossRef]
14. Loomis, T.P. Reaction of zoning of garnet. *Contrib. Mineral. Petrol.* **1975**, *52*, 285–305. [CrossRef]
15. Tracy, R.J. Compositional zoning and inclusions in metamorphic minerals. *Rev. Mineral. Geochem.* **1982**, *10*, 355–397.
16. Ikeda, T. Compositional zoning patterns of garnet during prograde metamorphism from the Yanai district, Ryoke metamorphic belt, Southwest Japan. *Lithos* **1993**, *30*, 109–121. [CrossRef]
17. Enami, M. Pressure-temperature path of Sanbagawa prograde metamorphism deduced from grossular zoning of garnet. *J. Metamorph. Geol.* **1998**, *16*, 97–106. [CrossRef]
18. Friend, C.R.L.; Nutman, A.P. New pieces to the Archaean terrane jigsaw puzzle in the Nuuk region, Southern West Greenland: Steps in transforming a simple insight into a complex regional tectonothermal model. *J. Geol. Soc. Lond.* **2005**, *162*, 147–162. [CrossRef]
19. Mcgregor, V.R.; Friend, C.R.L.; Nutman, A.P. The late Archaean mobile belt through Godthåbsfjord, Southern West Greenland: a continent-continent collision zone? *Bull. Geol. Soc. Denmark* **1991**, *39*, 179–197.
20. Komiya, T.; Maruyama, S.; Masuda, T.; Nohda, S.; Hayashi, M.; Okamoto, K. Plate Tectonics at 3.8–3.7 Ga: Field Evidence from the Isua Accretionary Complex, Southern West Greenland. *J. Geol.* **1999**, *107*, 515–554. [CrossRef] [PubMed]
21. Garde, A.A. *Accretion and Evolution of an Archaean High-Grade Grey Gneiss-Amphibolite Complex: The Fiskefjord Area, Southern West Greenland*; Geological Survey of Denmark and Greenland, Ministry of Environment and Energy: Copenhagen, Denmark, 1997.
22. Szilas, K.; van Hinsberg, V.; McDonald, I.; Næraa, T.; Rollinson, H.; Adetunji, J.; Bird, D. Highly refractory Archaean peridotite cumulates: Petrology and geochemistry of the Seqi Ultramafic Complex, SW Greenland. *Geosci. Front.* **2018**, *9*, 689–714. [CrossRef]
23. Sinton, J.M. Equilibration History of the Basel Alpine-Type Peridotite, Red Mountain, New Zealand. *J. Petrol.* **1977**, *18*, 216–246. [CrossRef]

24. Maurel, C.; Maurel, P. Étude expérimentale de la distribution de l'aluminium entre bain silicaté basique et spinelle chromifère. Implications pétrogénétiques: Teneur en chrome des spinelles. *Bull. Minéral* **1982**, *105*, 197–202.
25. Pearce, N.J.G.; Perkins, W.T.; Westgate, J.A.; Gorton, M.P.; Jackson, S.E.; Neal, C.R.; Chenery, S.P. A compilation of new and published major and trace element data for NIST SRM 610 and NIST SRM 612 glass reference materials. *Geostand. Geoanal. Res.* **1997**, *21*, 115–144. [CrossRef]
26. Longerich, H.P.; Jackson, S.E.; Günther, D. Inter-laboratory note. Laser ablation inductively coupled plasma mass spectrometric transient signal data acquisition and analyte concentration calculation. *J. Anal. At. Spectrom.* **1996**, *11*, 899–904. [CrossRef]
27. Morishita, T.; Arai, S.; Green, D.H. Evolution of Low-Al Orthopyroxene in the Horoman Peridotite, Japan: An Unusual Indicator of Metasomatizing Fluids. *J. Petrol.* **2003**, *44*, 1237–1246. [CrossRef]
28. Morishita, T.; Ishida, Y.; Arai, S.; Shirasaka, M. Determination of Multiple Trace Element Compositions in Thin (<30 um) Layers of NIST SRM 614 and 616 Using Laser Ablation-Inductively Coupled Plasma-Mass Spectrometry (LA-ICP-MS). *Geostand. Geoanal. Res.* **2005**, *29*, 107–122. [CrossRef]
29. Kelemen, P.B.; Hart, S.R.; Bernstein, S. Silica enrichment in the continental upper mantle via melt/rock reaction. *Earth Planet. Sci. Lett.* **1998**, *164*, 387–406. [CrossRef]
30. Larsen, J.G. Mantle-derived dunite and lherzolite nodules from Ubekendt Ejland, West Greenland Tertiary province. *Mineral. Mag.* **1982**, *46*, 329–336. [CrossRef]
31. Boyd, F.R.; Pokhilenko, N.P.; Pearson, D.G.; Mertzman, S.A.; Sobolev, N.V.; Finger, L.W. Composition of the Siberian cratonic mantle: evidence from Udachnaya peridotite xenoliths. *Contrib. Mineral. Petrol.* **1997**, *128*, 228–246. [CrossRef]
32. Bernstein, S.; Kelemen, P.B.; Brooks, C.K. Depleted spinel harzburgite xenoliths in Tertiary dykes from East Greenland: Restites from high degree melting. *Earth Planet. Sci. Lett.* **1998**, *154*, 221–235. [CrossRef]
33. Takahashi, E.; Uto, K.; Schilling, J.G. Primary Magma compositions and Mg/Fe ratios of their mantle residues along mid-atlantic ridge 29° N to 73° N. *Tech. Rep. ISEI Okayama Univ.* **1987**, *Ser. A*, 1–14.
34. Warren, J.M. Global variations in abyssal peridotite compositions. *Lithos* **2016**, *248–251*, 193–219. [CrossRef]
35. Khedr, M.Z.; Arai, S. Petrology and geochemistry of prograde deserpentinized peridotites from Happo-O'ne, Japan: Evidence of element mobility during deserpentinization. *J. Asian Earth Sci.* **2012**, *43*, 150–163. [CrossRef]
36. Arai, S. Contact metamorphosed dunite-harzburgite complex in the Chugoku district, Western Japan. *Contrib. Mineral. Petrol.* **1975**, *52*, 1–16. [CrossRef]
37. Nozaka, T.; Shibata, T. Mineral paragenesis in thermally metamorphosed serpentinites, Ohsa-yama, Okayama Prefecture. *Okayama Univ. Earth Sci. Rep.* **1995**, *2*, 1–11.
38. Sand, K.K.; Waight, T.E.; Pearson, D.G.; Nielsen, T.F.D.; Makovicky, E.; Hutchison, M.T. The lithospheric mantle below southern West Greenland: A geothermobarometric approach to diamond potential and mantle stratigraphy. *Lithos* **2009**, *112*, 1155–1166. [CrossRef]
39. Leake, B.E.; Woolley, A.R.; Arps, C.E.S.; Birch, W.D.; Gilbert, M.C.; Grice, J.D.; Hawthorne, Ec.; Kato, A.; Kisch, H.J.; Krivovichev, V.G.; et al. Nomenclature of amphiboles: report of the Subcommittee on Amphiboles of the International Mineralogical Association, Commission on New Minerals and Mineral Names. *Eur. J. Mineral.* **1997**, *9*, 623–651. [CrossRef]
40. Nozaka, T. Metamorphic history of serpentinite mylonites from the Happo ultramafic complex, Central Japan. *J. Metamorph. Geol.* **2005**, *23*, 711–723. [CrossRef]
41. Sun, S.-S.; McDonough, W.F. Chemical and isotopic systematics of oceanic basalts: Implications for mantle composition and processes. *Geol. Soc. Lond. Spec. Publ.* **1989**, *42*, 313–345. [CrossRef]
42. Bai, Y.; Su, B.-X.; Xiao, Y.; Lenaz, D.; Asamoah Sakyi, P.; Liang, Z.; Chen, C.; Yang, S.-H. Origin of Reverse Zoned Cr-Spinels from the Paleoproterozoic Yanmenguan Mafic-Ultramafic Complex in the North China Craton. *Minerals* **2018**, *8*, 62. [CrossRef]
43. Purvis, A.C.; Nesbitt, R.W.; Hallberg, J.A. The Geology of Part of the Carr Boyd Rocks Complex and Its Associated Nickel Mineralization, Western Australia. *Econ. Geol.* **1972**, *67*, 1093–1113. [CrossRef]
44. De Freitas Suita, M.T.; Strieder, A.J. Cr-Spinels from Brazilian Mafic-Ultramafic Complexes: Metamorphic Modifications. *Int. Geol. Rev.* **1996**, *38*, 245–267. [CrossRef]
45. Hamlyn, P.R.; Keays, R.R. Origin of chromite compositional variation in the Panton Sill, Western Australia. *Contrib. Mineral. Petrol.* **1979**, *69*, 75–82. [CrossRef]

46. Henderson, P.; Suddaby, P. The nature and origin of the chrome-spinel of the Rhum layered intrusion. *Contrib. Mineral. Petrol.* **1971**, *33*, 21–31. [CrossRef]
47. Henderson, P. Reaction trends shown by chrome-spinels of the Rhum layered intrusion. *Geochim. Cosmochim. Acta* **1975**, *39*, 1035–1044. [CrossRef]
48. Cameron, E.N. Postcumulus and subsolidus equilibration of chomite and coexisting silicates in the Eastern Bushveld Complex. *Geochim. Cosmochim. Acta* **1975**, *39*, 1021–1033. [CrossRef]
49. Hulbert, L.J.; Von Gruenewaldt, G. Textural and compositional features of chromite in the lower and critical zones of the Bushveld Complex south of Potgietersrus. *Econ. Geol.* **1985**, *80*, 872–895. [CrossRef]
50. Merinero, R.; Lunar, R.; Ortega, L.; Piña, R.; Monterrubio, S.; Gervilla, F. Zoned chromite records multiple metamorphic episodes in the Calzadilla de los Barros ultramafic bodies (SW Iberian peninsula). *Eur. J. Mineral.* **2014**, *26*, 757–770. [CrossRef]
51. Roeder, P.L. Chromite; from the fiery rain of chondrules to the Kilauea Iki lava lake. *Can. Mineral.* **1994**, *32*, 729–746.
52. Abzalov, M.Z. Chrome–spinels in gabbro–wehrlite intrusions of the Pechenga area, Kola Peninsula, Russia: Emphasis on alteration features. *Lithos* **1998**, *43*, 109–134. [CrossRef]
53. Barnes, S.J. Chromite in komatiites, II. Modification during greenschist to mid-amphibolite facies metamorphism. *J. Petrol.* **2000**, *41*, 387–409. [CrossRef]
54. Nozaka, T. Compositional heterogeneity of olivine in thermally metamorphosed serpentinite from Southwest Japan. *Am. Mineral.* **2003**, *88*, 1377–1384. [CrossRef]
55. Nozaka, T. A note on compositional variation of olivine and pyroxene in thermally metamorphosed ultramafic complexes from SW Japan. *Earth Sci. Rep. Okayama Univ.* **2010**, *17*, 1–5.
56. Arai, S.; Kida, M. Origin of fine-grained peridotite xenoliths from Iraya volcano of Batan Island, Philippines: Deserpentinization or metasomatism at the wedge mantle beneath an incipient arc? *Isl. Arc* **2000**, *9*, 458–471. [CrossRef]
57. Nakamura, Y.; Kushiro, I. Composition of the gas phase in $Mg_2SiO_4SiO_2$–H_2O at high pressures. In *Washington Yearbook*; Carnegie Institution of Washington: Washington, DC, USA, 1974; Volume 73, pp. 266–268.
58. Spear, F.S. *Metamorphic Phase Equilibria and Pressure-Temperature-Time Paths*; Mineralogical Society of America: Washington, DC, USA, 1993.
59. Arai, S.; Ishimaru, S. Insights into petrological characteristics of the lithosphere of mantle wedge beneath arcs through peridotite xenoliths: A review. *J. Petrol.* **2008**, *49*, 665–695. [CrossRef]
60. Payot, B.D.; Arai, S.; Tamayo, R.A.; Yumul, G.P. What underlies the Philippine island arc? Clues from the Calaton Hill, Tablas island, Romblon (Central Philippines). *J. Asian Earth Sci.* **2009**, *36*, 371–389. [CrossRef]
61. Green, D.H.; Ringwood, A.E. The genesis of basaltic magmas. *Contrib. Mineral. Petrol.* **1967**, *15*, 103–190. [CrossRef]
62. Presnall, D.C.; Dixon, S.A.; Dixon, J.R.; O'donnell, T.H.; Brenner, N.L.; Schrock, R.L.; Dycus, D.W. Liquidus phase relations on the join diopside-forsterite-anorthite from 1 atm to 20 kbar: Their bearing on the generation and crystallization of basaltic magma. *Contrib. Mineral. Petrol.* **1978**, *66*, 203–220. [CrossRef]
63. Borghini, G.; Fumagalli, P.; Rampone, E. The geobarometric significance of plagioclase in mantle peridotites: A link between nature and experiments. *Lithos* **2011**, *126*, 42–53. [CrossRef]
64. Milholland, C.S.; Presnall, D.C. Liquidus phase relations in the CaO-MgO-Al_2O_3-SiO_2 system at 3.0 GPa: The aluminous pyroxene thermal divide and high-pressure fractionation of picritic and komatiitic magmas. *J. Petrol.* **1998**, *39*, 3–27. [CrossRef]
65. Klemme, S.; O'Neill, H.S. The near-solidus transition from garnet lherzolite to spinel lherzolite. *Contrib. Mineral. Petrol.* **2000**, *138*, 237–248. [CrossRef]
66. Berman, R.G.; Engi, M.; Greenwood, H.J.; Brown, T.H. Derivation of Internally-Consistent Thermodynamic Data by the Technique of Mathematical Programming: A Review with Application the System MgO-SiO_2-H_2O. *J. Petrol.* **1986**, *27*, 1331–1364. [CrossRef]
67. Bucher, K.; Frey, M. Definition, Conditions and Types of Metamorphism. In *Petrogenesis of Metamorphic Rocks*; Springer: Berlin/Heidelberg, Germany, 2002; pp. 3–15.

68. Pearson, D.G.; Canil, D.; Shirey, S.B. Mantle samples included in volcanic rocks: Xenoliths and diamonds. *Treatise Geochem.* **2003**, *2*, 171–275.
69. Wittig, N.; Pearson, D.G.; Webb, M.; Ottley, C.J.; Irvine, G.J.; Kopylova, M.; Jensen, S.M.; Nowell, G.M. Origin of cratonic lithospheric mantle roots: A geochemical study of peridotites from the North Atlantic Craton, West Greenland. *Earth Planet. Sci. Lett.* **2008**, *274*, 24–33. [CrossRef]